Universal inverse design of surfaces with thin nematic elastomer sheets

Hillel Aharoni[a,1], Yu Xia[b,1], Xinyue Zhang[b], Randall D. Kamien[a], and Shu Yang[b,2]

[a]Department of Physics and Astronomy, University of Pennsylvania, Philadelphia, PA 19104; and [b]Department of Materials Science and Engineering, University of Pennsylvania, Philadelphia, PA 19104

Edited by Daan Frenkel, University of Cambridge, Cambridge, United Kingdom, and approved May 21, 2018 (received for review March 18, 2018)

Programmable shape-shifting materials can take different physical forms to achieve multifunctionality in a dynamic and controllable manner. Although morphing a shape from 2D to 3D via programmed inhomogeneous local deformations has been demonstrated in various ways, the inverse problem—finding how to program a sheet in order for it to take an arbitrary desired 3D shape—is much harder yet critical to realize specific functions. Here, we address this inverse problem in thin liquid crystal elastomer (LCE) sheets, where the shape is preprogrammed by precise and local control of the molecular orientation of the liquid crystal monomers. We show how blueprints for arbitrary surface geometries can be generated using approximate numerical methods and how local extrinsic curvatures can be generated to assist in properly converting these geometries into shapes. Backed by faithfully alignable and rapidly lockable LCE chemistry, we precisely embed our designs in LCE sheets using advanced top-down microfabrication techniques. We thus successfully produce flat sheets that, upon thermal activation, take an arbitrary desired shape, such as a face. The general design principles presented here for creating an arbitrary 3D shape will allow for exploration of unmet needs in flexible electronics, metamaterials, aerospace and medical devices, and more.

liquid crystal elastomers | inverse design | programmable shape shifting | click chemistry

A common modality of biological systems is the ability to shape themselves into various morphologies to interact with their surrounding environment, a concept also widely adopted by mankind in various technological contexts (1). Much effort has been invested in the last decades in the research of soft systems, that deform smoothly and continuously, often inspired by natural systems. Examples of such studies include, to name just a few, environmentally responsive hydrogels (2, 3), self-folding origami (4, 5) and kirigami (6), or smart textiles (7), with applications in soft robotics (8, 9), biomedicine (10–12), functional, and artistic design (13). In natural systems, the local structure often appears to be highly optimized for obtaining a certain shape that is necessary for fulfilling a certain function. Such high-end design is hard to achieve artificially, and biomimetics is often used to reproduce designs that appear in the natural world (14, 15). Still the question remains, how does one create a new stimulus-responsive design from scratch? How does the local structure at every point need to be set to get the desired global shape and response?

The answer depends on the local properties of the materials in use. For example, thin hydrogel sheets with programmable local isotropic expansion are widely studied in the context of shaping (2, 3). In these systems, the inverse design problem is mathematically well understood and generally solved (16). However, properties such as low elastic modulus, small deformations, slow response times, or the need for very specific aqueous environmental conditions may render such systems unsuitable for many applications. A class of materials that exhibit properties that are well suited for a wide range of design applications is liquid crystal elastomers (LCEs), that are lightly cross-linked polymer networks of liquid crystals (LCs). The inherent molecular anisotropy of LCs allows engineering the mechanical response of LCEs with fine control over both the magnitude and direction of the local strain. Compared with osmosis-driven hydrogel-based responsive materials, LCEs are characterized with high mechanical strength and quick response ($\sim 100\,ms$) (17), while exhibiting large anisotropic local deformations ($\sim 300\%$) in response to a variety of external stimuli (18), e.g., heat (19), light (20), or magnetic field (21). These materials have therefore been in the focus of much research in recent years, both theoretical and experimental (22). Since the anisotropic local deformation is different from the isotropic one, describing the local geometry of LCEs requires an entirely different mathematical framework than that used to describe isotropic materials systems such as hydrogels. Namely, it requires linking the geometry to the local molecular orientation—the nematic director—which is a principal axis of the local anisotropic deformation. The (forward) design problem for 2D LCE-type planar deformations (i.e., finding the geometry adopted by an LCE sheet upon stimulation given the predeformation nematic director field) is established in several recent theoretical works, both in a discrete framework (23, 24) and in a continuous one (25, 26).

This forward problem nonetheless foreruns the much harder inverse design problem—that is, finding a planar director field that would induce an arbitrary 2D geometry. The inverse problem was discussed in ref. 25 and later in ref. 15 but was not solved for the general case. Solutions were found for subclasses of the inverse problem—namely, when restricted to cases with radial or cylindrical symmetries (25, 27). In addition, general solutions were found for similar, less constrained inverse

Significance

This work outlines an explicit protocol for preprogramming any desired 3D shape into a 2D liquid crystal elastomer (LCE) sheet. Namely, given an arbitrary 3D design, we show how to produce a flat sheet that can buckle into the desired shape when heated and return to flat when cooled—reversibly. We demonstrate this proof-of-principle of shape morphing in LCE sheets, relying on advances in both numerical and experimental methods presented here. Our protocol is not limited in materials or scale; it can be implemented on any "LCE-like" anisotropic material, thus opening the door for countless technological applications in flexible electronics, metamaterials, aerospace, medical devices, drug delivery, and more.

Author contributions: H.A., Y.X., R.D.K., and S.Y. designed research; H.A., Y.X., and X.Z. performed research; H.A. and Y.X. contributed new reagents/analytic tools; H.A., Y.X., X.Z., R.D.K., and S.Y. analyzed data; and H.A., Y.X., R.D.K., and S.Y. wrote the paper.

The authors declare no conflict of interest.

This article is a PNAS Direct Submission.

See Commentary on page 7171.

[1]H.A. and Y.X. contributed equally to this work.

[2]To whom correspondence should be addressed. Email: shuyang@seas.upenn.edu.

This article contains supporting information online at www.pnas.org/lookup/suppl/doi:10.1073/pnas.1804702115/-/DCSupplemental.

Published online June 21, 2018.

problems—namely, when relaxing the planar-field demand and assuming full control over the 3D director field at every point (28) or when relaxing the demand for homogeneous nematic-order parameter and polymer properties, thus assuming full local control over all components of the planar deformation and curvature tensors (29). However, experimental realization of those assumptions will be extremely challenging. This is in contrast to planar-director LCEs, for which many experimental methods have been investigated, aiming to improve the accuracy and spatial resolution of the nematic director field at every point. Initial attempts to construct both smooth curvature fields and discrete ones proved successful (26, 30–32), and recent work demonstrated the ability to make general radially symmetric designs (33).

While these works lay the cornerstone for realizing truly arbitrary designs of thin LCE sheets, there still remain several obstacles before reaching this goal; first, the general inverse design problem for planar fields is yet unresolved; second, assuming a solution exists, one needs to be able to accurately and faithfully imprint it onto a thin LCE sheet and obtain the correct local stimulus-responsive deformation in practice; and third, obtaining the right 2D geometry is not enough since it can have many different isometric embeddings in space and since the system might end up being dynamically stuck in a nonisometry or in an otherwise undesired configuration. Therefore, control over additional degrees of freedom needs be achieved in order for these methods to be applied for general designs.

In this work, we resolve some of these issues in an attempt to allow the design of arbitrarily shaped surfaces from flat LCE sheets, implementing several theoretical and experimental techniques. We first take a numerical approach in approximating a solution to the inverse design problem, thus obtaining a planar nematic director field that equips the sheet with the desired 2D metric tensor. We realize these designs using a variation on the top-down microfabrication technique that was previously developed by some of the authors (32) to precisely control the molecular orientation at every point in the LCE sheet. Combined with LCE polymer chemistry based on a "click" reaction that can efficiently and faithfully produce uniform strain across the film (34), we create a high-accuracy realization of the theoretical designs with precise control over both the direction and magnitude of the local strain in the polymer films. Furthermore, we incorporate higher-order techniques to better ensure buckling of the sheet toward the correct isometry and avoid stagnation at local equilibria away from the desired design. Specifically, we introduce local reference curvatures for the components of the target curvature tensor which can be achieved with a strictly planar director field. We show how the combination of these methods allows us to create sheets that upon activation take an arbitrary design (e.g., a face) (Fig. 1).

Results and Discussion

Numerical Inverse Design of 2D Geometries. The mathematical formulation of the inverse design problem for thin planar nematic elastomer plates was presented in ref. 25. It involves, given a desired 2D metric tensor $\bar{a}$, finding coordinates $\{u, v\}$ and a director field $\theta(u, v)$, so that $\bar{a}$ takes the form

$$\bar{a}(u,v) = R\left[\theta(u,v)\right]\begin{pmatrix}\lambda^2 & 0\\ 0 & \lambda^{-2\nu}\end{pmatrix}R\left[\theta(u,v)\right]^T. \qquad [1]$$

Here, λ and $\lambda^{-\nu}$ are the local expansion ratios parallel and perpendicular to the nematic director field, respectively, and $R[\theta]$ is the planar rotation matrix by angle θ. Following ref. 25, the problem can be equivalently posed as finding coordinates $\{u, v\}$ in which, at every point, the Jacobian of the mapping from coordinate space to the desired surface has singular values $\{\lambda, \lambda^{-\nu}\}$.

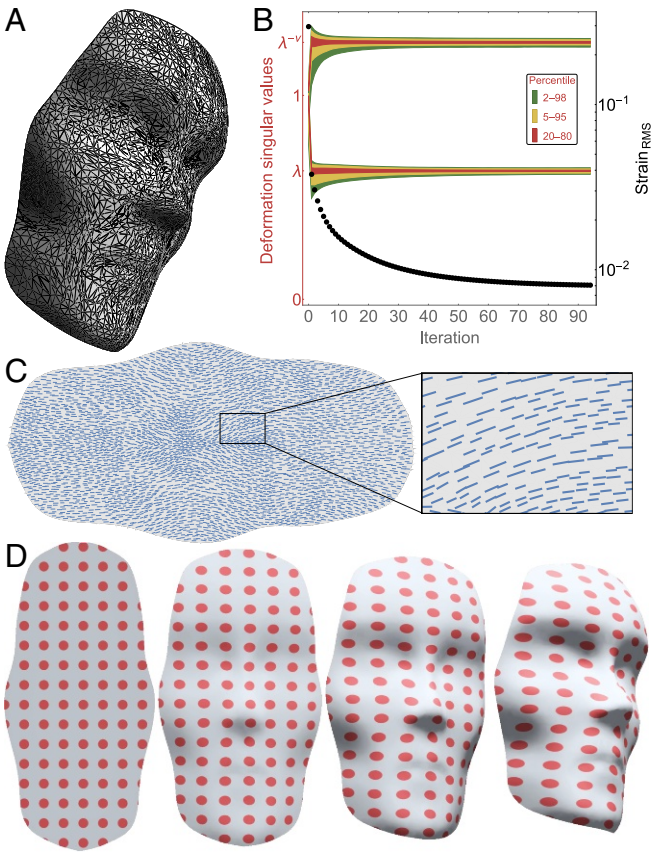

Fig. 1. Numerical inverse design of arbitrary geometry. (*A*) The input for our numerical algorithm is a surface in 3D, given in the form of a triangulated mesh with some initial 2D parameterization. (*B*) Distribution of singular values (left scale) of the individual triangles' deformation from the plane to the surface (percentiles in orange). As the algorithm iteratively changes the parameterization, all singular values approach the target values $\{\lambda, \lambda^{-\nu}\}$. The residual strain (right logarithmic scale) between the target metric and our constructed metric Eq. **1** diminishes (black circles). (*C*) As output, our algorithm assigns to each triangle 2D coordinates and a director angle (blue segments). The deformation between every plane-triangle and its matching surface-triangle approximates the anisotropic material deformation at the target temperature. (*D*) The deformation visualized with Tissot's indicatrices. Circles in the undeformed planar domain (*Left*) map onto the deformed surface as ellipses, with constant temperature-dependent principal axes $\{\lambda, \lambda^{-\nu}\}$ and with principal directions aligned along the calculated local director. At the target λ, the desired surface is reconstructed (*Right*).

We took a numerical approach for finding an approximate solution to this problem. We started with a desired surface given as a triangulated mesh in 3D and with certain values of λ and ν that described material deformation at a certain desired temperature (Fig. 2*C*). Our goal—the discrete equivalent of Eq. **1**—was to assign to each vertex a set of 2D coordinates, such that the linear transformation from 2D to 3D of every mesh triangle had singular values $\{\lambda, \lambda^{-\nu}\}$. We started with some initial 2D coordinate parameterization, which we iteratively modified to obtain good approximations of the target singular values at every triangle (Fig. 1*B*). Our algorithm for this procedure was based on a numerical algorithm presented in ref. 35 and involved within each iteration a set of local singular value decompositions followed by solving one global linear set of equations. We describe the algorithm in further detail in *SI Appendix*.

Once the algorithm converged, we had as output a 2D coordinate mesh, $\{u, v\}$, with the same triangulation as the input surface, along with a director angle θ defined at each mesh

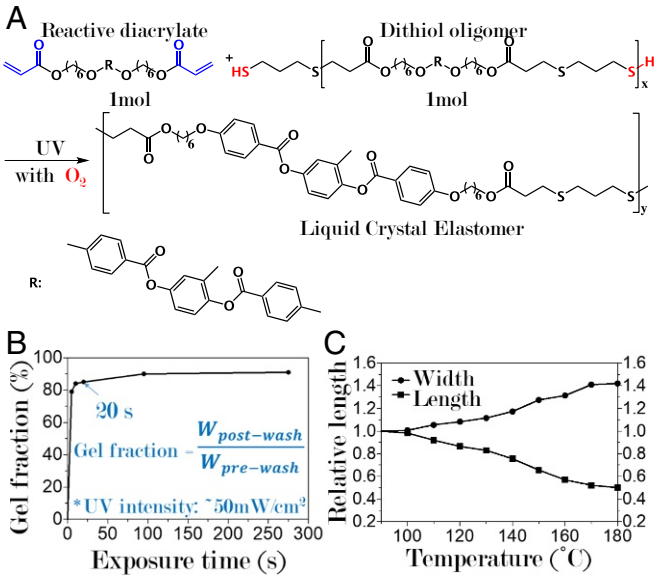

Fig. 2. Characterization of thiol-acrylate click reaction for precise control of local strain in LCEs. (*A*) Schematic of the thiol-acrylate click reaction. (*B*) Polymerization speed of the reaction measured by using the gel fraction of the LCE film exposed to UV at different exposure times. (*C*) Deformation of uniformly aligned free LCE film, in the directions parallel and perpendicular to the director, as a function of temperature.

triangle. The intrinsic 2D geometry of such a sheet was expected to follow Eq. **1**; hence, it was Euclidean at preparation temperature ($\lambda_{\text{prep}} = 1$) and approximated the geometry of our desired surface upon accepting the target values of λ and ν. We evaluated the approximation error, which is the strain between the geometry of the target surface and the metric [**1**]. When necessary, we refined the mesh or ran the algorithm starting at a different initial condition until the two metrics were essentially the same; therefore, we had an approximate solution to the inverse problem for the given surface [even though the existence of an exact solution remains unproven (25)]. For all of the surfaces that were tested, a solution with root-mean-square metric error of $<1\%$ was found.

Experimental Realization. To realize the designs given by our numerical algorithm, it was crucial to prepare spatially heterogeneous LCEs with precisely controlled lateral deformation at every point. It thus required control not only of the arbitrary position-dependent orientation of the nematic director, but also of the magnitude of local principal strains throughout the film. Since the theory and numerical algorithm assumed constant principal strains $\{\lambda^2, \lambda^{-2\nu}\}$ across the film, it was necessary to fulfill this requirement in the real experimental system. However, traditional LCE photopolymerization chemistry (36) is based on free radical polymerization, which seriously suffers from the inhibition reaction of oxygen from the ambient air. Not only does this require a long UV curing time that generates excess heat that can alter the LC alignment, but it also creates a nonuniform cross-linking density across the film, which in turn would affect the local strain in the film. To overcome this challenge, we developed a surface-alignable LCE chemistry based on an oxygen-mediated thiol-acrylate "click" reaction (Fig. 2*A* and ref. 34), allowing for immediate locking of the LC director field in the local domains.

This should be done with caution, however; mixing of a fraction of nonmesogenic reactant, such as dithiols, into the mesogenic LC could destroy the liquid crystalline order (37) by altering the packing of the mesogens. To suppress this effect, we prepared LCEs via a two-step synthetic procedure. First, we prepolymerized mesogenic diacrylates {1,4-bis-[4-(6-acryloyloxy-hexyloxy)benzoyloxy]-2-methylbenzene (RM82)} and nonmesogenic dithiol (1,3-propane dithiol) via a base-catalyzed click reaction to generate a mesogenic dithiol oligomer mixture of various chain lengths (*SI Appendix*, Fig. S2). After reaction, the dithiol oligomer was in a nematic phase at room temperature and could be homogenously mixed with RM82 at any fraction ratio without destroying the nematic phase. The mixture had an extremely large nematic window of $\sim 118^\circ C$ (*SI Appendix*, Fig. S3*A*).

We then obtained the LCEs through photopolymerization of the RM82/dithiol oligomer mixture. In the polymerization process, the reaction between thiols and acrylates that generates linear polymer chains competed with the homopolymerization of acrylates that produces cross-linking sites (38). Here, by carrying out the reaction in the presence of air, we used the inhibition of homopolymerization by oxygen from the ambient air to suppress the unwanted cross-linking reactions (39, 40), which was critical to ensure the formation of a low cross-linking density LCE rather than an LC glass. It turned out that the thiol-acrylate reaction was extremely efficient, leading to 85% gelation after only 20-s UV irradiation at $50\ mW/cm^2$ (Fig. 2*B*). The process resulted in polymer films with highly uniform cross-linking density (41), allowing a faithful execution of our protocol that requires uniform λ and ν throughout the sheet.

After cross-linking, we ended up with a low modulus and low glass transition temperature elastomer (*SI Appendix*, Figs. S3*B* and S4). The LCE film showed clear birefringence and shape changes in response to heating (*SI Appendix*, Fig. S5*A*). We prepared a uniformly aligned LCE film to measure the variation in the length and width of the film upon heating and calculated the thermo-responsive strain plotted in Fig. 2*C* and *SI Appendix*, Fig. S5*B*. The maximum strain of our LCE system was found to be $\sim 100\%$ in the system of RM82/dithiol oligomer at $1:1$ ratio of functional group. These large values of λ granted access to a wide variety of 2D geometries via our numerical algorithm. The value of ν was close to $1/2$ at all temperatures.

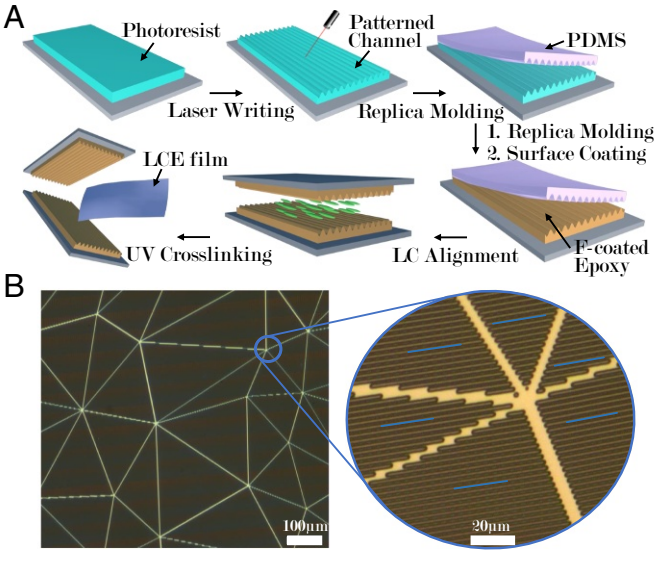

Fig. 3. Achieving accurate control over local deformation. (*A*) Experimental procedure. (*B*) An optical microscope image of channels patterned onto the epoxy-coated glass mold for controlling the local alignment of the planar nematic director field. Individual channels are visible in the further magnified *Inset*, where channel orientation in each monolithic domain is denoted by the blue segments.

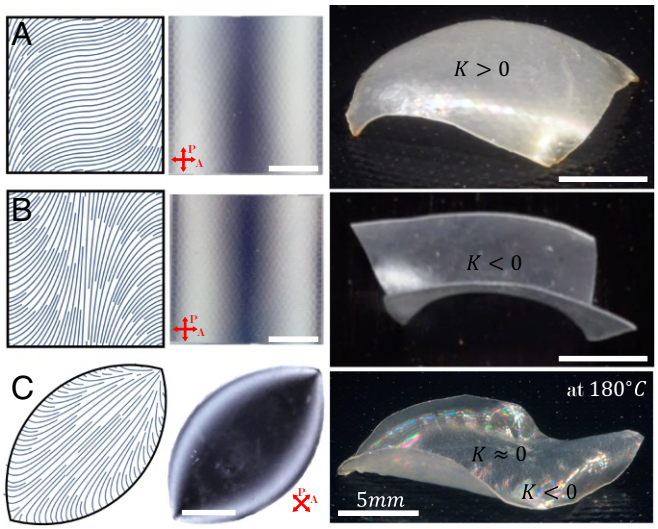

Fig. 4. Designing simple shapes using only their 2D geometry. (*Left*) The theoretically or numerically obtained planar director fields are imprinted onto the LCE sheet. (*Center*) We measure the experimentally obtained director field using crossed polarizers to verify that it coincides with the desired field. (*Right*) When brought to the target temperature 180°*C*, the initially flat LCE sheet takes the desired 3D shape. The procedure is shown for the following geometries: constant positive Gaussian curvature (*A*), constant negative Gaussian curvature (*B*), and leaf-shaped surface, with strong negative Gaussian curvature around the sides (*C*). (Scale bars: 5 mm.)

Spatial control over the nematic director field has been demonstrated in photoalignment systems (31) and in our previously reported photo-patterned 1D channel system (32) (with feature size 2 μm). Here, we implemented our method to align LCs according to our numerical designs. To further improve the alignment quality, we used a photo-patterning technique through direct laser writing (see details in *SI Appendix*) to prepare an even smaller pattern feature size of 1 μm that gives a much higher surface anchoring energy (42) (see detailed discussion in *SI Appendix*). We prepared channel-patterned molds with channel width of 1 μm, spacing of 1 μm, and depth of 600 nm, arranged into monolithic domains of average size ∼200–500 μm (Fig. 3*B* and *SI Appendix*, Fig. S6), corresponding to the discrete elements in our numerical algorithm. The two sides of the mold were placed with a 150-μm spacing between them, into which we capillary infiltrated the RM82/dithiol oligomer melt. The nematic director locally aligned with channel direction, and fast UV cross-linking trapped it inside the solid LCE films (Fig. 3*A*). We used this system to realize designs obtained by our numerical algorithm, with good success in reproducing several simple designs. Some of these are shown in Fig. 4—surfaces of constant positive and negative Gaussian curvatures (which can be thought of as building blocks for arbitrary 2D geometries) and the shape of a leaf with negative Gaussian curvature exponentially decaying away from the edge (43). In *SI Appendix*, Fig. S7, we further characterize the positive Gaussian curvature surface, comparing the measured curvature and the theoretical prediction at different temperatures. The curvatures agree well at lower temperatures, but deviate at temperatures $\geq 150^\circ C$ on account of several adverse effects. A detailed explanation can be found in *SI Appendix*.

Inducing Reference Curvature. As we attempted to produce more complex models (e.g., the face in Fig. 1, whose 2D geometry consists of smaller length scales and alternating curvatures), we faced more challenges. One reason for this might be that with such geometries, the thin limit assumption is less valid, and bending energy plays a bigger role trying to locally flatten the sheet. Considering the size of our monolithic domains ∼200–500 μm as a lower bound on the radii of curvature in our designs, we alleviated this problem by decreasing the film thickness to 100 μm to approach the thin limit; however, with the mechanical integrity of the LCE film in mind, we refrained from going lower. Another problem with complex designs is the abundance of different isometries and near-isometries of the desired shape, which is further aggravated by the dynamic process in which different regions in our sample might initially buckle in different directions and be left stuck away from the system's global ground state.

To grapple with these issues, we introduced nontrivial local reference curvatures in the sheet by augmenting our designs with a small gradient in the nematic director across the sheet's thickness. The inflicted nematic twist broke the up–down symmetry of the sheet—namely, making the top side slightly shorter than the bottom side along its director and vice versa. This mechanism, along with an explicit calculation of the induced reference curvature tensor, is described in ref. 25. As explained there, it cannot be used to create any desired local curvature; with strictly planar anchoring, one can only induce a reference curvature tensor with equal and opposite principal curvatures, with principal curvature directions at $\pm 45^\circ$ with respect to the thickness-averaged director. This implies an unavoidable mismatch between the induced curvature and metric tensors,

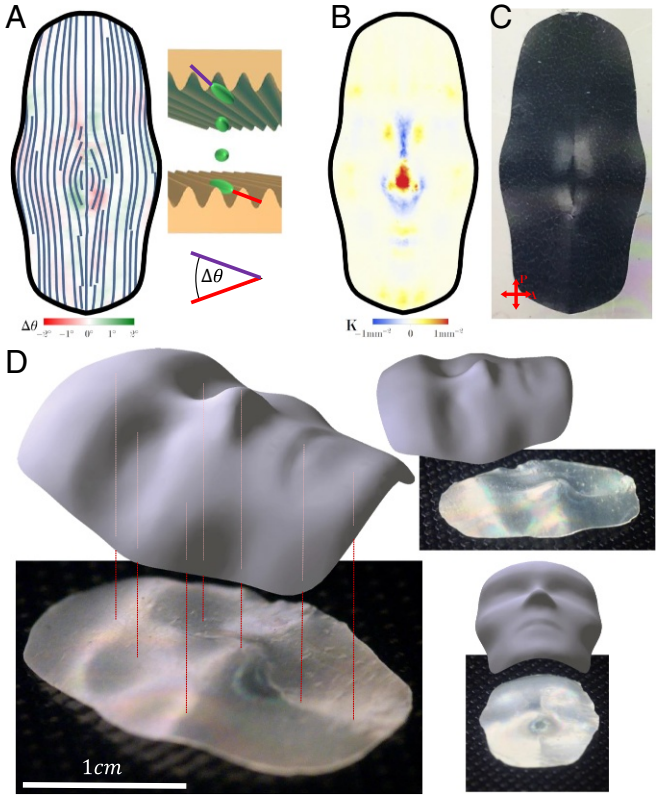

Fig. 5. Designing a face using both metric tensor and curvature tensor. (*A*) Two slightly different director fields are imposed on the top and bottom surfaces of the LCE sheet. Shown streamlines indicate the director field at the midplane, while color indicates the angle difference $\Delta\theta$ between the top and bottom (illustrated by *Inset* sketch). (*B*) Gaussian curvature of the target surface. The correlation between regions with strong negative Gaussian curvature and regions with strong $|\Delta\theta|$ stems from the saddle-like form of the induced curvature tensor. (*C*) Polarized optical microscopy is used to verify the resulting director field throughout the LCE sheet. (*D*) At the target temperature 180°*C* the LCE sheet takes the shape of a face.

which results in residual elastic energy that only vanishes in the infinitely thin limit. The only additional scalar-field degree of freedom one has in inducing the reference curvature is the absolute value of the principal curvatures, which is proportional to the magnitude of the local director field gradient at every point (25). We calculated the value of this scalar field $\Delta\theta(u, v)$ that minimized the discrepancy between the induced reference curvature and the curvature of the desired shape. A detailed calculation can be found in *SI Appendix*. The output of the numerical calculation was values of $\Delta\theta$ evaluated at each mesh triangle. This gave us for each mesh triangle two director fields: $\theta + \Delta\theta/2$ for the top surface of the sheet and $\theta - \Delta\theta/2$ for the bottom surface. Since the difference between these two fields was small (in our models $|\Delta\theta| \lesssim 5^\circ$) and continuous, the nematic strain caused by it was not enough to compromise surface anchoring or to promote nematic defects, nor did it significantly change the induced reference metric (see discussion in *SI Appendix*).

We realized such a director field by creating two independent channel patterns for the top and bottom parts of the mold, instead of using two mirror images of the same pattern. We still used the same triangulated mesh for both sides, only the channels within each monolithic domain were oriented in slightly different directions (Fig. 5*A*). The resulting director field remained essentially planar throughout the sample and twisted smoothly from top to bottom to match the direction of the channels on both sides. When heated, the reference curvatures caused the resulting LCE film to buckle in the desired direction at certain areas, thus pushing it dynamically toward the preferred isometry—a face (Fig. 5*D* and *SI Appendix*, Fig. S8). The process was completely reversible, and multiple heating/cooling cycles switched the sample between flat and face-shaped configurations repeatedly (at least 30 cycles, as seen in *SI Appendix*, Fig. S9).

This work brings together numerical and experimental methods to address a universal inverse problem—that is, how to reconstruct 3D surfaces from 2D sheets of anisotropic LCEs. We established an explicit protocol for preprogramming any desired shape into an LCE sheet. Our protocol is not limited in material or scale; LCs are not necessarily molecular; they can be any material with long-range orientational order, and an LCE-like anisotropic material could be any LC coupled with any elastic medium. Our designs can therefore be broadly used in systems ranging from cellulose nanocrystals embedded in polymer networks to sewing threads embedded in hydrogels. This allows the design of shape-shifting surfaces at a wide variety of length scales and material properties, which, combined with the shape-universality of our design scheme, opens the door for countless technological applications.

Materials and Methods

A detailed account of the methods described below can be found in *SI Appendix*.

Numerical Methods. Our numerical procedure, executed in Matlab (code is provided in *SI Appendix*), accepted as input the target shape as a triangulated surface in 3D and material parameters at the target temperature. The first step, calculating 2D coordinates for each vertex and a planar director angle for each triangle to induce the 2D metric of the target surface, was an adaptation of the mesh parameterization local/global algorithm (35). The second step, calculating a director angle gradient across the thickness to induce preferable local curvatures, was a straightforward projection of the target surface's curvature tensor on directions diagonal to the director calculated in the first step. We then had, for each planar mesh triangle, one director angle for the top surface and one for the bottom surface. This data were used later for patterning the top and bottom surfaces of the epoxy LC cell.

Preparation of LCE Sheets. LCEs were prepared following the procedures reported in refs. 32 and 34. Dithiol oligomer was synthesized by reacting RM82 and 1,3-propanedithiol at 1:2 molar ratio, with 1,8 diazabicycloundec-7-ene serving as a catalyst. Then, a mixture of liquid crystal monomer (LCM) precursor consisting of 1:1 molar ratio of RM82 and the as-prepared dithiol oligomer was heated into isotropic phase (100°C) and infiltrated into a prepatterned epoxy LC cell, within which both top and bottom surfaces were designed with 1D channels for the alignment of LCM, according to our numerical algorithm. The LC cell was then subjected to a UV irradiation at a dosage of 10^3 to 10^4 mJ/cm^2 to fully cure the LCM. The final LCE film was obtained by opening the LC cell with a razor blade and slowly peeling off the membrane from the epoxy patterns. The LCE film was then transferred to a hot plate for the study of shape deformation under heating and cooling.

ACKNOWLEDGMENTS. This work was supported by National Science Foundation (NSF) DMR/Polymer Program Grant DMR-1410253 (to S.Y.). This work is also partially supported by NSF/Emerging Frontiers in Research and Innovation–Origami Design for Integration of Self-Assembling Systems for Engineering Innovation (EFRI-ODISSEI) Grant 13-31583, NSF Grant DMR-1262047, and a Simons Foundation Simons Investigator grant (to R.D.K.).

1. Burgert I, Fratzl P (2009) Actuation systems in plants as prototypes for bioinspired devices. *Philos Trans R Soc A Math Phys Eng Sci* 367:1541–1557.
2. Klein Y, Efrati E, Sharon E (2007) Shaping of elastic sheets by prescription of non-Euclidean metrics. *Science* 315:1116–1120.
3. Kim J, Hanna JA, Byun M, Santangelo CD, Hayward RC (2012) Designing responsive buckled surfaces by halftone gel lithography. *Science* 335:1201–1205.
4. Tolley MT, et al. (2014) Self-folding origami: Shape memory composites activated by uniform heating. *Smart Mater Struct* 23:094006.
5. Na J-H, et al. (2015) Programming reversibly self-folding origami with micropatterned photo-crosslinkable polymer trilayers. *Adv Mater* 27:79–85.
6. Zhang Y, et al. (2015) A mechanically driven form of Kirigami as a route to 3D mesostructures in micro/nanomembranes. *Proc Natl Acad Sci USA* 112:11757–11764.
7. Hu J, Meng H, Li G, Ibekwe SI (2012) A review of stimuli-responsive polymers for smart textile applications. *Smart Mater Struct* 21:053001.
8. Shepherd RF, et al. (2011) Multigait soft robot. *Proc Natl Acad Sci USA* 108:20400–20403.
9. Trivedi D, Rahn CD, Kier WM, Walker ID (2008) Soft robotics: Biological inspiration, state of the art, and future research. *Appl Bionics Biomech* 5:99–117.
10. Woltman SJ, Jay GD, Crawford GP (2007) Liquid-crystal materials find a new order in biomedical applications. *Nat Mater* 6:929–938.
11. Fernandes R, Gracias DH (2012) Self-folding polymeric containers for encapsulation and delivery of drugs. *Adv Drug Deliv Rev* 64:1579–1589.
12. Randall CL, Gultepe E, Gracias DH (2012) Self-folding devices and materials for biomedical applications. *Trends Biotechnol* 30:138–146.
13. Ritter A (2007) *Smart Materials: In Architecture, Interior Architecture and Design* (Birkhäuser, Basel), p 191.
14. Ionov L (2013) Biomimetic hydrogel-based actuating systems. *Adv Funct Mater* 23:4555–4570.
15. Gladman AS, Matsumoto EA, Nuzzo RG, Mahadevan L, Lewis JA (2016) Biomimetic 4D printing. *Nat Mater* 15:413–418.
16. Chern SS (1955) An elementary proof of the existence of isothermal parameters on a surface. *Proc Am Math Soc* 6:771–782.
17. Camacho-Lopez M, Finkelmann H, Palffy-Muhoray P, Shelley M (2004) Fast liquid-crystal elastomer swims into the dark. *Nat Mater* 3:307–310.
18. Ohm C, Brehmer M, Zentel R (2010) Liquid crystalline elastomers as actuators and sensors. *Adv Mater* 22:3366–3387.
19. Thomsen DL, et al. (2001) Liquid crystal elastomers with mechanical properties of a muscle. *Macromolecules* 34:5868–5875.
20. Finkelmann H, Nishikawa E, Pereira G, Warner M (2001) A new opto-mechanical effect in solids. *Phys Rev Lett* 87:015501.
21. Kaiser A, Winkler M, Krause S, Finkelmann H, Schmidt AM (2009) Magnetoactive liquid crystal elastomer nanocomposites. *J Mater Chem* 19:538–543.
22. Warner M, Terentjev EM (2003) *Liquid crystal elastomers*, International Series of Monographs on Physics (Oxford Univ Press, Oxford), Vol 120, p 423.
23. Modes CD, Bhattacharya K, Warner M (2010) Disclination-mediated thermo-optical response in nematic glass sheets. *Phys Rev E* 81:060701.
24. Modes CD, Warner M (2011) Blueprinting nematic glass: Systematically constructing and combining active points of curvature for emergent morphology. *Phys Rev E* 84:021711.
25. Aharoni H, Sharon E, Kupferman R (2014) Geometry of thin nematic elastomer sheets. *Phys Rev Lett* 113:257801.
26. Mostajeran C, Warner M, Ware TH, White TJ (2016) Encoding Gaussian curvature in glassy and elastomeric liquid crystal solids. *Proc R Soc Lond A Math Phys Eng Sci* 472:20160112.
27. Warner M, Mostajeran C (2018) Nematic director fields and topographies of solid shells of revolution. *Proc R Soc A Math Phys Eng Sci* 474:20170566.
28. Plucinsky P, Lemm M, Bhattacharya K (2016) Programming complex shapes in thin nematic elastomer and glass sheets. *Phys Rev E* 94:010701.
29. van Rees WM, Vouga E, Mahadevan L (2017) Growth patterns for shape-shifting elastic bilayers. *Proc Natl Acad Sci USA* 114:11597–11602.

30. De Haan LT, Sánchez-Somolinos C, Bastiaansen CMW, Schenning APHJ, Broer DJ (2012) Engineering of complex order and the macroscopic deformation of liquid crystal polymer networks. *Angew Chem Int Ed* 51:12469–12472.
31. Ware TH, McConney ME, Wie JJ, Tondiglia VP, White TJ (2015) Voxelated liquid crystal elastomers. *Science* 347:982–984.
32. Xia Y, Cedillo-Servin G, Kamien RD, Yang S (2016) Guided folding of nematic liquid crystal elastomer sheets into 3D via patterned 1D microchannels. *Adv Mater* 28:9637–9643.
33. Kowalski BA, Mostajeran C, Godman NP, Warner M, White TJ (2018) Curvature by design and on demand in liquid crystal elastomers. *Phys Rev E* 97:012504.
34. Xia Y, Zhang X, Yang S (2018) Instant locking of molecular ordering in liquid crystal elastomers by oxygen-mediated thiol-acrylate click reactions. *Angew Chem Int Ed* 57:5665–5668.
35. Liu L, Zhang L, Xu Y, Gotsman C, Gortler SJ (2008) A local/global approach to mesh parameterization. *Eurogr Symp Geom Process* 27:1495–1504.
36. Broer DJ, Crawford GP, Žumer S (2011) *Cross-Linked Liquid Crystalline Systems: From Rigid Polymer Networks to Elastomers* (CRC, Boca Raton, FL), p 586.
37. Ware TH, Perry ZP, Middleton CM, Iacono ST, White TJ (2015) Programmable liquid crystal elastomers prepared by thiol–ene photopolymerization. *ACS Macro Lett* 4:942–946.
38. Ki Kim S, Guymon CA (2012) Effects of polymerizable organoclays on oxygen inhibition of acrylate and thiol-acrylate photopolymerization. *Polymer (Guildf)* 53:1640–1650.
39. Cramer NB, Bowman CN (2001) Kinetics of thiol-ene and thiol-acrylate photopolymerizations with real-time Fourier transform infrared. *J Polym Sci A Polym Chem* 39:3311–3319.
40. O'Brien AK, Cramer NB, Bowman CN (2006) Oxygen inhibition in thiol–acrylate photopolymerizations. *J Polym Sci Part A Polym Chem* 44:2007–2014.
41. Hoyle CE, Bowman CN (2010) Thiol-ene click chemistry. *Angew Chem Int Ed* 49:1540–1573.
42. Berreman DW (1972) Solid surface shape and the alignment of an adjacent nematic liquid crystal. *Phys Rev Lett* 28:1683–1686.
43. Sharon E, Roman B, Swinney HL (2007) Geometrically driven wrinkling observed in free plastic sheets and leaves. *Phys Rev E* 75:46211–46217.